Weathering profiles, mass-balance analysis, and rates of solute loss: Linkages between weathering and erosion in a small, steep catchment

Suzanne Prestrud Anderson*
Center for Study of Imaging and Dynamics of the Earth, University of California, Santa Cruz, California 95064-1077, USA

William E. Dietrich
George H Brimhall Jr.
Department of Earth and Planetary Sciences, University of California, Berkeley, California 94720-4767, USA

ABSTRACT

In a headwater catchment in the Oregon Coast Range, we find that solid-phase mass losses due to chemical weathering are equivalent in the bedrock and the soil. However, the long-term rate of mass loss per unit volume of parent rock is greater in the soil than in the rock. We attribute this finding to the effects of biotic processes in the soil and to hydrologic conditions that maximize contact time and water flux through the mineral matrix in the soil. This result stems both from earlier work in which we demonstrated that rock and soil contribute equally to the solute flux and from arguments presented here that the basin is in dynamic equilibrium with respect to erosion and uplift. The silica flux of 10.7 ± 7.1 $t \cdot km^{-2} \cdot yr^{-1}$ from the basin is several times larger than the flux from older soils elsewhere, but comparable to the flux from sites with similar physical erosion rates. This result argues that physical denudation or uplift rates play an important role in setting the chemical denudation rate. Physical processes appear to influence chemical-weathering rates in several ways. First, they limit chemical evolution by removing material, thus setting the residence time within the weathered rock and the soil. Second, bioturbation mixes rock fragments into the more reactive soil and maintains high soil porosity, allowing free circulation of water. Because the weathering in the soil is more intense than in the rock, we argue that the chemical denudation rate will diminish where uplift rates—and, hence, physical-denudation rates—are great enough to lead to a bedrock-dominated landscape. Chemical denudation rates will increase with physical-denudation rates, but only as long as the landscape remains mantled by soil.

Keywords: chemical erosion, denudation, physical weathering, soil dynamics, uplift, weathering.

INTRODUCTION

The weathered profile, consisting of layers of weathered rock topped by soil, develops in response to chemical, physical, and biological processes at the Earth's surface. The strong interplay among these processes makes it difficult to disentangle their interactions in the weathered profile. Physical weathering processes expose fresh rock and mineral surfaces to chemical weathering, whereas chemical weathering reduces the strength of rock, making it more susceptible to physical breakdown. The interactions between these processes are widely recognized as critical in understanding the effects of changes in climate and of tectonic uplift rates on erosion (Raymo et al., 1988), landscape evolution (Anderson and Humphrey, 1989), and geochemical cycling (Gaillardet et al., 1999a).

The balance between removal of debris by transport processes and the breakdown of rock into movable material by weathering exerts a strong control on landscape evolution. G.K. Gilbert (1877) described the linkage between regolith production and erosion rates, now codified by geomorphologists who differentiate conceptually between weathering-limited and transport-limited landscapes (Carson and Kirkby, 1972). In the former, the rate of formation of erodible debris by physical and chemical processes controls the rate of landscape lowering. Landscapes dominated by bare bedrock are universally recognized as weathering-limited. In contrast, landscapes with deep regolith mantles are transport-limited. The rate of landscape lowering is limited by the efficiency of transport processes, and the weathered profile thickens through time. Stallard (1985) demonstrated that these concepts could be used to explain the evolution of chemical loads of large rivers.

Recent empirical advances (Heimsath et al., 1997, 1999, 2000, 2001a) support the concept that regolith-production rates decline under increasing soil cover. In an alternative model, regolith production reaches a maximum under a particular soil depth and is reduced under both shallower and deeper soil cover (Ahnert, 1967; Carson and Kirkby, 1972; Stallard, 1985; Anderson and Humphrey, 1989; Rosenbloom and Anderson, 1994; Small et al., 1999). Mechanistic justification for either type of production rule is usually couched in terms of the effects of increasing soil depth on chemical and/or thermomechanical (Anderson, 1999) processes.

Understanding the interplay between physical and chemical weathering processes and their relationship to erosion rates has become increasingly important in understanding geochemical cycles (Stallard, 1992, 1995b). The potential feedbacks between erosion and chemical weathering were brought to prominence by the erosion-driven climate change hypothesis (Raymo et al., 1988; Raymo and Ruddiman, 1992). Given that global silicate-

*E-mail: spa@earthsci.ucsc.edu.

GSA Bulletin; September 2002; v. 114; no. 9; p. 1143–1158; 9 figures; 3 tables.

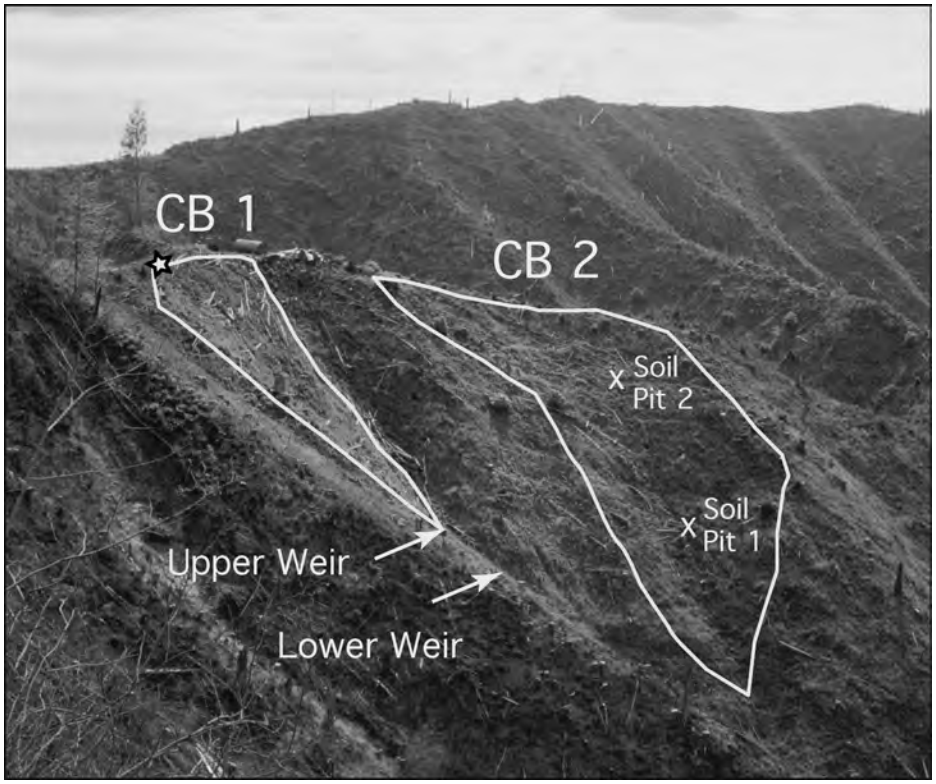

Figure 1. Photograph of the CB1 and CB2 catchments and surrounding hillslopes. View is to the southwest, oblique to the north-facing CB1 catchment. CB1 catchment is 50 m long and ~20 m wide near the ridge crest. CB2 is 95 m long and ~45 m wide. Soil pits were located in CB2 to avoid disturbance to CB1. Star shows location of deep core (Fig. 2).

weathering rates exert an important control on the long-term C dioxide content of the atmosphere (Holland, 1978; Berner, 1990), if silicate chemical weathering is linked to physical denudation and tectonic uplift (Ruddiman and Prell, 1997), then weathering and erosion may drive climate change. A number of workers have stressed the importance of physical erosion in enhancing chemical-weathering rates (Stallard, 1992, 1995a; Gaillardet et al., 1999a, 1999b; Riebe et al., 2001), whereas White and Blum (1995) found little correlation between chemical weathering and physical erosion rates. The relationship between physical processes and chemical weathering has not been elucidated at a mechanistic level, but this mission is most likely to be accomplished in a small catchment, where there is more control on rock type, vegetation, and local climate.

We present here a detailed study of the weathered profile in a headwater catchment in the Oregon Coast Range (Fig. 1) and of the processes that have shaped it. We use chemical analyses of soil and bedrock as well as prior work on soil water chemistry (Anderson et al., 1997a; Anderson and Dietrich, 2001) and catchment hydrology (Montgomery et al., 1997; Anderson et al., 1997b; Torres et al., 1998). Previously, we have shown that half of solutes exported from the catchment are produced in the soil and half in the bedrock. Here, we quantify solid-phase mass gains and losses in the weathered profile, and we determine the time for weathered-profile development. This approach allows us to compare the long-term rate of mass loss in the bedrock and soil.

The field site does not represent extremes of either physical or chemical weathering conditions. Instead, one expects both relatively vigorous physical processes (owing to the site's steep slopes and active tectonics) and active chemical weathering (driven by the moderately heavy rainfall). Biological influences on weathering processes are both physical and chemical in nature and are well expressed in the catchment. Climate variation since the Pleistocene has been relatively modest (Worona and Whitlock, 1995); hence, current processes are similar to those that shaped the landscape. The uplift rate in the Oregon Coast Range drives sufficient erosion to keep the soils relatively thin, but is not so high as to produce large tracts without appreciable soil development. The rainfall rate is high enough to produce measurable weathering in the rock and soil during their relatively brief transit through the weathered zone.

Our exploration of weathered-profile development takes several tacks. First, we describe the weathered profile and its spatial variation. A chemical mass-balance technique (Brimhall and Dietrich, 1987) allows quantification of the mass gains and losses of individual chemical elements relative to fresh parent rock. Second, we compare the alteration of the rock with measured solute fluxes from the catchment, permitting comparison of present-day weathering processes with time-integrated chemical losses from the bedrock. We can then quantify the rate of mass loss due to weathering in the bedrock and in the soil. Together, these analyses show that physical processes open the bedrock up to hydrologic processes and drive the production of soil. Chemical processes attack the rock vigorously once it is in contact with air, rainwater, and the biosphere, but this activity must be viewed as a consequence of the environment produced by physical processes.

Setting

The study site is the 860 m^2 CB1 catchment, located in the Oregon Coast Range near Coos Bay, Oregon (Fig. 1). Topography of the Oregon Coast Range is marked by steep hillslopes bounded by bedrock and gravel channels. Alluvial fills are confined to narrow valleys along the coast inundated by late Holocene sea-level rise (Personius, 1993; Personius et al., 1993). Uplift of rock beneath the Coast Range (Adams, 1984; Kelsey et al., 1994) continually generates steep topographic gradients to drive incision of streams and erosion of hillslopes. The record preserved in marine terraces yields rock-uplift rates of 0.03–0.23 $mm \cdot yr^{-1}$ over the past 80–125 ka along the southern Oregon coast (Kelsey et al., 1994, 1996), probably ~0.1 $mm \cdot yr^{-1}$ in the vicinity of Coos Bay (H. Kelsey, 1994, personal commun.).

Soils are thin in the Coast Range, but soil depth varies considerably. Erosion rates over the southern Oregon Coast Range have been 0.05–0.08 $mm \cdot yr^{-1}$ for the past 4–15 ka (Reneau and Dietrich, 1991; Reneau et al., 1989), roughly equivalent to the long-term uplift rates. Reneau and Dietrich (1991) found that bedrock-lowering rates (also called ''exhumation rates'' by England and Molnar, 1990),

determined from colluvium in-filling rates of unchanneled valleys in the Oregon Coast Range, were equal to sediment yield in streams. The equivalence of denudation rates across spatial scales from 1 to 1500 km^2 suggests that there are no changes in sediment storage in the system. Recent catchment-averaged regolith-production rates of 0.117 mm·yr^{-1} (Heimsath et al., 2001b) also match uplift and denudation rates. Heimsath et al. found considerable variability in regolith-production rates over a small spatial scale (meters to tens of meters), however, which they attributed to both the stochastic nature of the biogenic processes that form the regolith and the effects of local competition between drainage networks and episodic erosional events. At scales greater than these variations, however, the landscape appears to be in dynamic equilibrium, and uplift rates are equal to denudation rates.

Catchment Description

The CB1 catchment is an unchanneled valley, a basin with convergent bedrock topography that forms the contributing area to a first-order stream (Fig. 1). The outlet of the CB1 catchment is the head of an ephemeral first-order stream. The steep (45°) slopes of the catchment are thinly mantled with soil, which supported a Douglas fir (*Pseudotsuga menzeisii*) forest until the area was logged in 1987. It was replanted in 1988. The catchment is underlain by the Eocene Flournoy Formation, a rhythmically bedded graywacke sandstone containing quartz, feldspar, and lithic (volcanic) fragments in a matrix of clay minerals (Baldwin, 1974, 1975).

The CB1 catchment and the adjacent, slightly larger CB2 catchment were monitored hydrologically from December 1989 to February 1992 (CB2) or November 1996 (CB1). Monitoring ended in both cases because of landslides. Sprinkling experiments were mounted in CB1 to study the hydrology and water chemistry in the runoff (Anderson et al., 1997a, 1997b; Montgomery et al., 1997; Torres et al., 1998).

METHODS

Spatial variations in the weathered profile were documented by coring, hand augering, and digging soil pits. A 35-m-long, 65-mm-diameter core was obtained at the top of the CB1 catchment with a truck-mounted drill rig. Core recovery averaged 93% below the upper 3 m, which were air blasted without recovery. The channel head is located ~42 m below the catchment divide, and the sandstone beds dip no more than 8°–15°S into the slope. This core is therefore representative of the bedrock underlying most of CB1 and CB2. Eleven shallow bedrock borings within the catchment were made with a portable diamond-bit corer (MacDonald, 1988); these cores generally had poor recovery, but pieces up to 0.5 m long helped characterize bedrock at points within the catchment. About 100 holes were hand-augered in the catchment to delineate the soil and saprolite thickness. Examination of exposures of the soil/bedrock interface in landslide scars also contributed to our understanding of the spatial differences in weathered-profile development.

Twenty samples were taken from the 35 m core to characterize the unweathered parent material and the weathered rock. Fourteen soil samples were collected with a piston corer in two soil pits in the CB2 catchment (Fig. 1). CB1 and CB2 soils are comparable, as they are derived from the same bedrock and are at a similar stage in the hollow-filling cycle (Dietrich et al., 1986).

Rock bulk densities were determined by water displacement of wax-coated samples (average size, 72 cm^3). Soil bulk densities were determined for oven-dried piston core samples. Grain-density determinations were made with a pycnometer on milled rock or disaggregated soil. Rock and soil samples were prepared for chemical analysis by producing pulps with a disc mill. Determinations of Al, Ti, Mg, Ca, Na, K, and Fe were done on La_2O_3 solutions of HF-digested samples with a Perkin-Elmer 3030 flame atomic adsorption spectrometer. Determinations of Si and Zr were done with XRF (X-ray fluorescence) spectrometry (Spectrace 440) on fused and pressed pellets, respectively. C and N were analyzed with a Perkin-Elmer Model PE2400 CHNS/O analyzer.

Thin sections of six samples from the core and two samples from the soil pits were point-counted to document the mineral assemblage. Quartz was distinguished from feldspar on the basis of twinning, which may have resulted in an undercounting of feldspar grains (our quartz counts are higher than those that Lovell (1969) and Dott (1966) obtained in formations similar to the Flournoy).

Soil waters were sampled with 34 suction lysimeters and two zero-tension lysimeters during a February 1992 winter storm with a three-day total rainfall of 144 mm, and during a catchment-scale sprinkling experiment (experiment 3) in May–June 1992. Peak runoff during the storm was 10 times greater than during the sprinkling experiment. For experiment 3, a nearly steady ''rain'' of 1.6 mm·h^{-1} (38 mm·d^{-1}) was applied over the entire catchment for one week. The intensity was selected to typify storms in the region; it is equivalent to a 24 h event with $<$1 yr recurrence interval (Montgomery et al., 1997). Analysis of daily rainfall for two years shows that daily rainfall totals $\geq$38 mm occur in ~10% of annual rain days (National Climate Data Center [http://lwf.ncdc.noaa.gov/oa/ncdc.html] records for North Bend Airport). In 1983 (annual rainfall 150% of normal), days with $\geq$38 mm rain accounted for 26% of the annual total, while in 1992 (annual rainfall 92% of normal), days with $\geq$38 mm rain accounted for 16% of the annual total. Experiment 3 was long enough that quasi-steady flow conditions were reached in the soil and outlet channel (Anderson et al., 1997b; Torres et al., 1998).

Soil water samples were field filtered (0.45 μm) and analyzed for cations and silica by inductively coupled plasma–mass spectrometry and for anions by ion chromatography (see Anderson and Dietrich, 2001, for details). Alkalinity was measured by titration with 0.1*N* HCl by using the Gran method. ''Organic anions'' were estimated from the difference between cation and anion concentrations (Dahlgren and Ugolini, 1989).

RESULTS

The Weathered Profile

We divided the weathered profile into four layers based on differences in physical properties, fractures, and degree of weathering (Fig. 2). There is great contrast, chiefly in bulk density (Fig. 3) and organic C content, between soil and bedrock. Saprolite is present spottily in the catchment. We identified two layers within the weathered bedrock below the saprolite. The predominant lithology in the unweathered rock is fine-grained graywacke. Minor calcite-cemented graywacke was associated with faults and fractures.

The soil in the CB1 catchment is classified as Haplumbrept by the Soil Conservation Survey (Haagen, 1989), reflecting its limited pedogenic development. The soil is an extremely porous (average bulk density of 740 ± 190 kg·m^{-3}) sandy loam. It is also organic rich; C content averages 2.5 wt%, and reaches as high as 10 wt% in the surface litter (Anderson and Dietrich, 2001). The soil surface is hummocky owing to the presence of tree-throw mounds and the spoils and tunnels of burrowing animals. The boundary between soil and bedrock is abrupt. A thin layer of saprolite underlies the soil in some areas in the catchment. The saprolite is orange to tan in color and lacks

organic material. The fact that it is penetrable with a hand auger or shovel implies that weathering has substantially weakened it. The bulk densities of the two samples we collected were 1850 and 1150 kg·m^{-3}.

The weathered bedrock below the saprolite can be divided into two layers. Bulk density is not a discriminator; it varied by only 60 kg·m^{-3} around an average of 2270 kg·m^{-3} throughout the core (Fig. 3). We use oxidized color and fracture density to subdivide the weathered rock into pervasively oxidized and fractured, partially oxidized rock layers. Open fractures, often stained with Fe or Mn oxides, increase in frequency toward the surface, where horizontal fractures occurred in addition to high-angle fractures (Fig. 2). Veins decrease in frequency toward the surface and were equally likely to have calcite or silica fillings or linings. Most of the veins and fractures were steeply inclined (45°–80° from horizontal) and are probably tectonic in origin. Horizontal fractures were observed in the top 3 m of the core.

The pervasively oxidized rock layer extends to a depth of 4.5 m below the surface, which is approximately the upper extent of pyrite preservation. Pyrite, the most reactive mineral in the parent material, is a good indicator of oxidation processes and related acid generation. Core recovery was ~70%, and the rock was highly broken up over this interval. All of the rock recovered was tan to orange in color, and the surfaces of fractures, many of which were horizontal, were coated with brown to orange oxidized material. The transition to the fractured and partially oxidized rock layer was rather abrupt at 4.5 m depth, and this layer extended to ~9 m. Core recovery was nearly 100%. Open fractures in this layer were stained and surrounded with oxidation bands up to 25 mm thick. The rock was competent and unoxidized between fractures and outside the oxidation halos.

Below 9 m depth, the rock was essentially unweathered. Oxidation stains were seen on some fracture faces, but oxidation halos in the surrounding sandstone were absent. Few horizontal fractures were seen. Two fractures were notable below 9 m depth. An open fracture with Fe and Mn oxide stains on its surfaces at 22 m depth was associated with shale

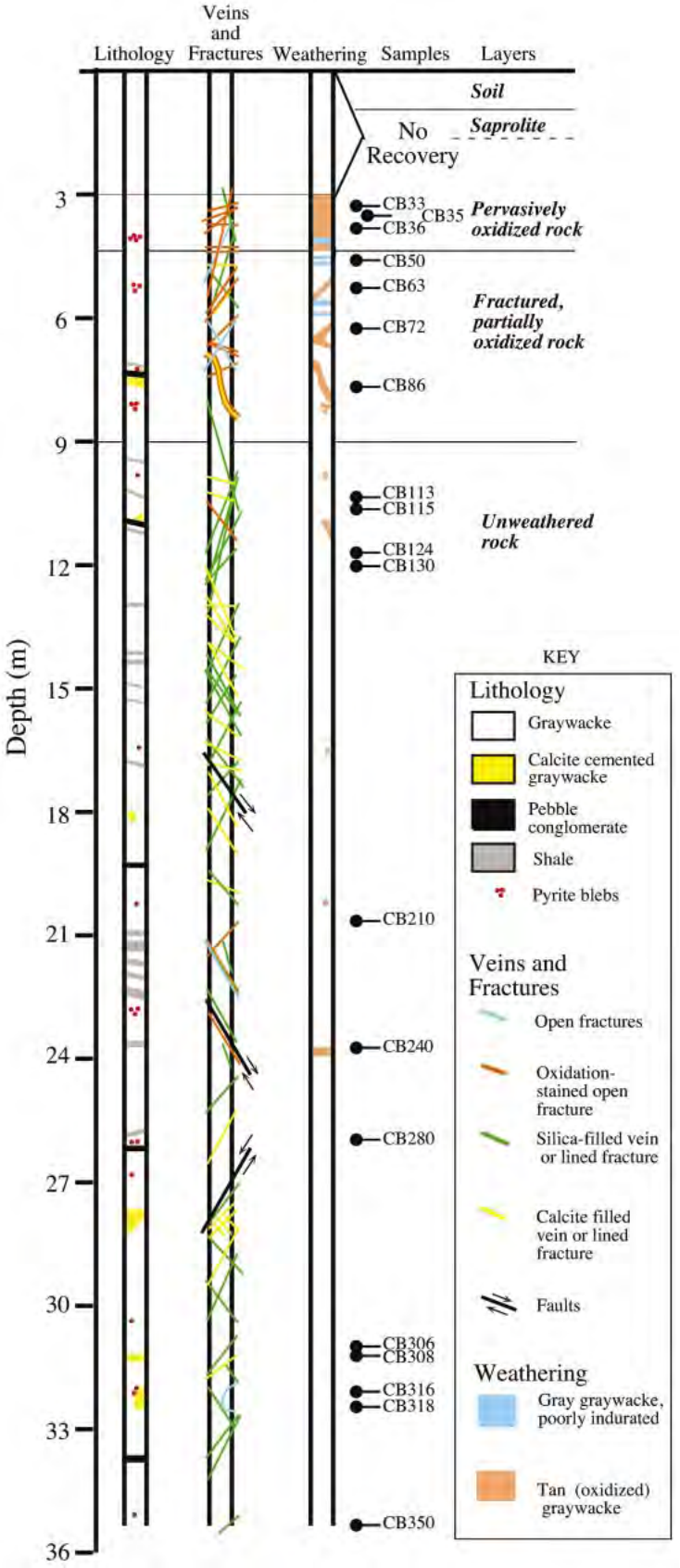

Figure 2. Log of the 35 m core, showing variations in lithology, fractures and veins, and weathered appearance. Rock sample locations shown with filled circles. The top 3 m were air blasted without recovery.

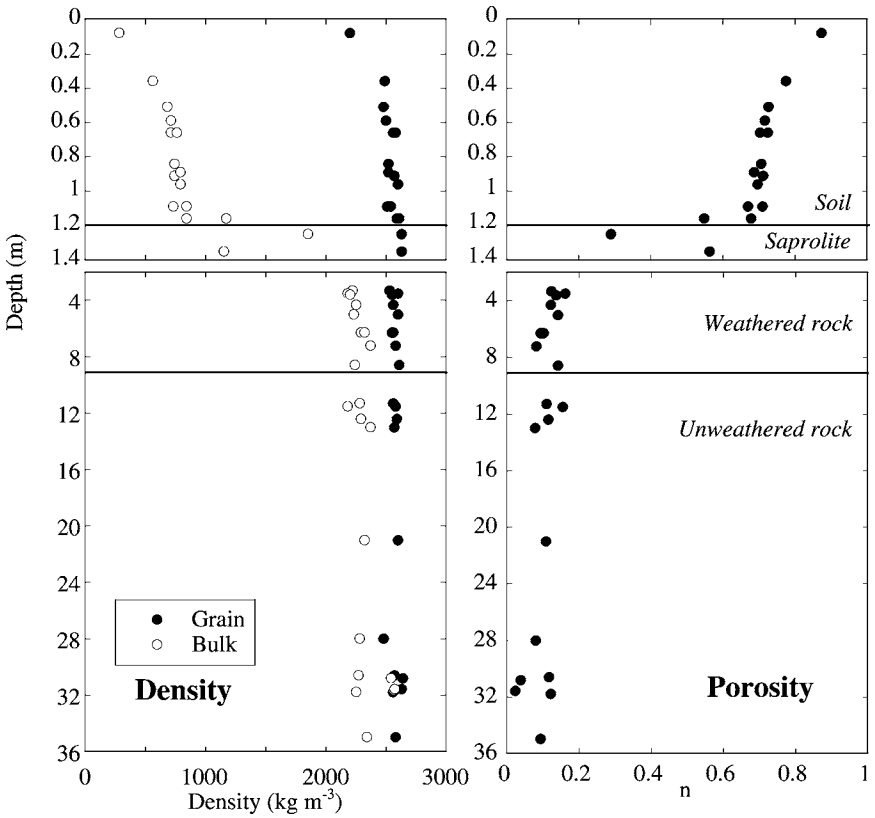

Figure 3. Bulk density, grain density, and porosity as a function of depth in soil and bedrock. Note the vertical-scale break below the saprolite layer; samples in the upper box are from soil pits 1 and 2 in CB2; samples below this are from the core in CB1 (Fig. 1).

beds. More oxidation was evident along a fault at 24 m depth. Below these features, all the rock was competent and gray in color, and no oxidation stains were seen.

Spatial Variation in Weathered-Profile Development

All of the weathered layers in the bedrock become thinner downslope (Fig. 4). The soil thickens downslope, reaching a maximum ~15 m above the channel head. Cross sections at right angles to the longitudinal profile show the soil accumulations in the hollow. Average soil depth is 0.70 ± 0.41 m (n = 104). Saprolite is present as a nearly continuous layer in the top third of the catchment. It is thin or missing under the deepest soil in the hollow axis in the lower third of the catchment, probably owing to removal in periodic landsliding events. The saprolite varies tremendously in thickness where it is found (0.23 ± 0.26 m, n = 36, excluding borings with no saprolite). The variations in saprolite thickness found on the east nose are suggestive of blocky core stone-style weathering and are consistent with observations of Heimsath et al. (2001b) and with patterns seen in roadcuts.

Mineral Assemblage Variations

The mineral assemblage of the graywacke parent material is dominated by quartz, feld-

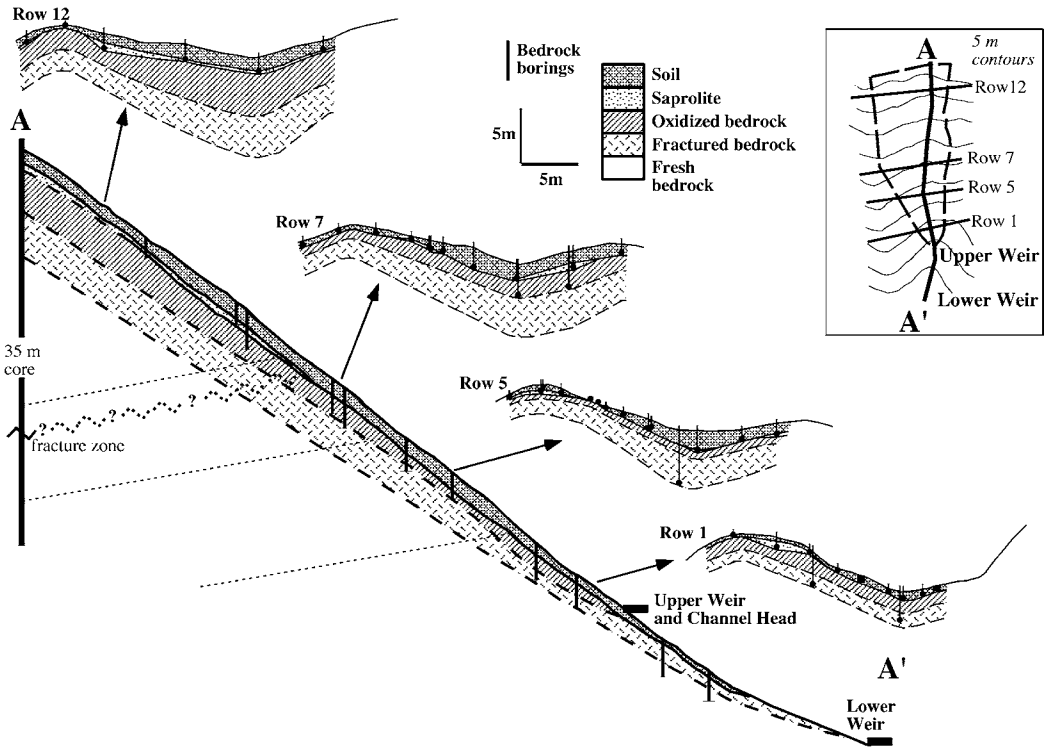

Figure 4. Longitudinal profile and cross sections of the catchment, without vertical exaggeration. The boundaries of weathered-rock layers are extrapolated between tie points of the 35 m core at the top of the profile and bedrock borings indicated with vertical lines. Access rows across the site are numbered consecutively from bottom to top; cross sections at a few representative rows are shown.

spar, and lithic (volcanic) fragments in a fine-grained groundmass (Table 1). A decline in plagioclase and an increase in reddish groundmass are the primary differences between the parent rock and the pervasively oxidized rock. Variation between the parent-rock samples is as great as any variation within the weathered profile for mica, lithic, hornblende, or alkali feldspar contents. Pitted and weathered quartz and plagioclase grains are evident throughout the core, but are present in greater abundance in oxidized rock samples. Fractures were lined with reddish-colored groundmass in the pervasively oxidized rock layer (thin sections CB33 and CB35), and the mineral grains edging the fractures were more likely to be pitted than those in unfractured parts of the thin section. In these weathered-rock samples, a high-birefringence groundmass appeared to coat many mineral grains, especially those lining fractures.

In the soil samples, quartz, feldspar, biotite, and volcanic-glass abundances were lower than in the rock, whereas reddish groundmass and void spaces were more common. The ratio of quartz to plagioclase increased by a factor of three to five. The groundmass was uniformly reddish in color and, in places, was nearly opaque because of either organic material or oxides. All mineral grains within rock fragments in the soil were pitted and embayed, and overgrowths were common. Plagioclase was found in the soil, but it was much less abundant than in the fresh parent rock.

WHOLE-ROCK CHEMISTRY: QUANTIFICATION OF WEATHERING ALTERATION

Mass-Balance Model

We quantified elemental losses and gains that accompany weathering in the soil and rock through the use of a chemical mass-balance model (Brimhall et al., 1985, 1991, 1992; Brimhall and Dietrich, 1987). The model is predicated on identification and characterization of the parent rock. Physical deformation, or strain, accompanying weathering can be calculated by conserving the mass of an element that is unaffected by chemical weathering. Thus, both the chemical transformations and physical deformation of weathering can be quantified with this simple model.

The mass of a chemical element, j, in a volume of weathered material, V_w, is equal to the mass of the element in the volume of fresh parent rock, V_p, that weathered to produce V_w and the mass of the element added or lost in the weathering process, $m_{j,\mathrm{flux}}$:

$$\frac{1}{100}(V_w \rho_w C_{j,w}) = \frac{1}{100}(V_p \rho_p C_{j,p}) + m_{j,\mathrm{flux}}, \quad (1)$$

where ρ is the bulk density, C_j is the concentration in weight percent of element j, and the subscripts w and p refer to weathered material and parent rock, respectively. In order to quantify the mass gains or losses associated with weathering, the volume changes that accompany weathering must be known. For an element that is immobile during weathering, and that does not have an external source, the $m_{j,\mathrm{flux}}$ term of equation 1 is zero. In this case, equation 1 can be solved for the volumetric strain, $\varepsilon_{i,w}$, of the weathered material relative to the parent rock:

$$\varepsilon_{i,w} = \frac{V_w}{V_p} - 1 = \frac{\rho_p}{\rho_w}\frac{C_{i,p}}{C_{i,w}} - 1. \quad (2)$$

Here the subscript i replaces j to emphasize that equation 2 applies only for an immobile element.

The strain from equation 2 can be used to calculate mass gains or losses due to weathering from equation 1. These are expressed as absolute mass changes per unit volume of parent rock, $\delta_{j,w}$, with units of mass per unit volume:

$$\delta_{j,w} \equiv \frac{m_{j,\mathrm{flux}}}{V_p} = \frac{1}{100}\left(C_{j,w}\rho_p\frac{C_{i,p}}{C_{i,w}} - \rho_p C_{j,p}\right) \quad (3)$$

or as percent mass changes relative to the mass of the element in parent rock with the dimensionless element-mass-transfer coefficient, $\tau_{j,w}$:

$$\tau_{j,w} \equiv \frac{m_{j,\mathrm{flux}}}{V_p \rho_p C_{j,p}} 100 = \frac{C_{j,w} C_{i,p}}{C_{j,p} C_{i,w}} - 1. \quad (4)$$

Equations 3 and 4 show explicitly the dependence of these calculated mass gains and losses on elemental concentrations and parent-rock density. Errors in measurements of soil bulk density propagate only into the calculation of strain (equation 2) and not into the calculation of mass gains and losses (equations 3 and 4).

Addition of material to the soil surface through eolian deposition is a possible source of error in the mass-balance analysis. We think that eolian inputs are not likely to be significant in the CB1 soil given the long distance from Asian dust sources, the relatively wet climate (minimizing local sources), and the young age of the soils.

Mass-Balance Model Results

We used three of the deepest samples from the core to define parent material. The three samples (CB306, CB318, and CB350; see Fig. 2 and Table 1) are from >5 m below the permanent water table at 25 m and are composed of competent graywacke lacking visible oxidation. The average chemical composition of these samples defined the $C_{j,p}$ and $C_{i,p}$ terms in all calculations. Strains within the soil calculated by assuming Ti and Zr immobility describe a nearly perfect 1:1 relationship; in the calculations that follow we use Zr as the immobile element.

TABLE 1. MINERALOGY OF SELECTED SAMPLES

	Parent rock			Pervasively oxidized rock			Soil	
Sample:	CB350	CB318	CB306	CB43	CB35	CB33	Pit1	Pit2
Sample depth (m)	35.0	31.8	30.6	4.3	3.5	3.3	0.3	0.6
Points counted	200	100	90	100	100	100	100	100
Quartz	40	52	40	44	39	40	32	35
Plagioclase	14	15	13	8	3	6	2	2
Alkali feldspar	3	4	0	2	1	1	0	0
Lithic	7	8	14	13	5	9	4	6
Biotite	6	1	6	3	5	4	2	2
Hornblende	3	3	1	2	4	3	0	4
Muscovite	0	3	1	0	2	2	2	0
Glass (volcanic)	6	1	2	2	15	0	0	0
Opaque	1	2	0	0	0	2	0	2
Groundmass	20	11	17	14	15	24	21	43
Reddish groundmass*	0	0	6	11	11	6	36	26
Void†	1	0	0	1	0	6	53	54
Quartz/plagioclase	2.9	3.5	3.1	5.5	13.0	6.3	15.0	16.0

Note: All mineral abundances reported as percent of nonvoid points.
*Organic matter or oxides.
†Percentage of total points that were voids.

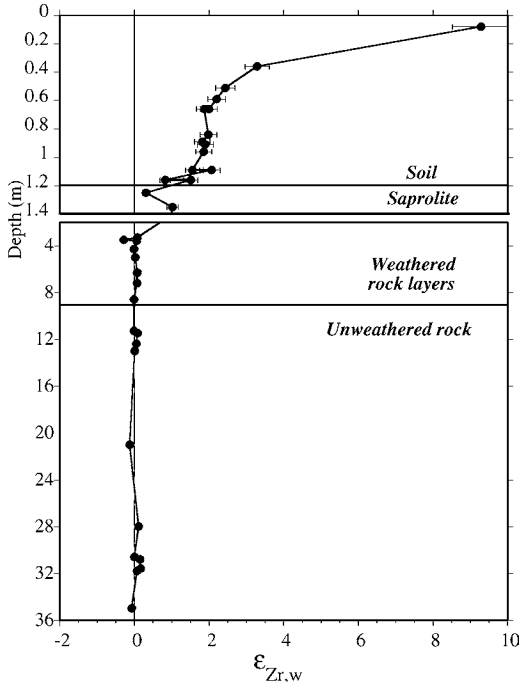

Figure 5. Profile of volumetric strain, ε, in the soil and weathered-rock layers. Strain is calculated from equation 2 by assuming Zr immobility; error bars show the variations due to the range of parent-material composition. Note the depth-scale break below the saprolite.

Soil and bedrock are dramatically different in their physical properties (Fig. 3). Soil bulk densities are less than half those of bedrock, and porosities are correspondingly large. The decline in bulk density arises from formation of porosity. Consequently, the measured strain is large and positive in the soil, but essentially zero within the rock (Fig. 5). The saprolite samples show positive strains that are intermediate between deep soil and rock. Most of the soil has undergone a positive strain of ~2: i.e., a parcel of rock expands by 100% when converted into soil.

Variability in the parent-rock composition leads to some uncertainty in the mass-balance calculations. In Figure 6, shaded swaths show the effect of compositional differences between the three parent-rock samples on $\tau_{j,w}$. Only values that fall outside of this swath can be considered different from the parent rock. This uncertainty is greatest for Al and Si, because of the large variations in their concentrations in the parent rock and their small percentage changes through the weathered profile.

The mass transfers of individual elements are greatest within the soil (Fig. 6). Up to 50% of the Ca and 25% of the Mg and Na originally present in the rock has been removed from the soil. The calculated mass transfers of Si in the soil do not fall outside the range of variability in the parent rock, except for the shallowest sample. Nonetheless, all $\tau_{Si,w}$ values within the soil are negative, rather than distributed about zero, suggesting that silica has been lost from the soil, but the depletions are at the limits of detection with this method. If the silica data are taken at face value, they amount to ~10% loss in the soil relative to the parent rock. C (and N—not shown, but well correlated with C) both show dramatic gains in the soil, reflecting organic matter accumulation. K, which is biologically cycled, shows a slight accumulation in the shallowest soil sample that probably reflects transport up into plants and redeposition in leaf litter on the soil surface (note the association of positive $\tau_{K,w}$ with an extremely high C addition). K retention in the soil follows from the preservation of muscovite in at least one soil pit (Table 1). Al and Fe show slight mass gains in the soil profile, although as with Si, the mass transfers for these elements do not rise above the parent-rock variability. Our parent-rock samples appear anomalously low in Al. Nearly all samples in the profile, including all but one of the unweathered-rock samples, show Al additions relative to the parent material. The absolute mass changes in the soil are summarized in Figure 7, which shows that in absolute terms, mass losses rank Si > Ca > Na ≥ Mg, whereas C dominates the mass gains. Both soil pits yield a total mass loss within the soil column of ~100 kg·m^{-2}.

The two saprolite samples stand out from both the soil and the weathered rock (Fig. 6). Both samples have Ca and Na losses comparable to those of the overlying soil, but lack the slight silica losses and significant C additions of the soil. There are accumulations of Al and K in the saprolite not seen elsewhere. We tentatively attribute these to translocation of these elements from the soil because of podzolization. In contrast, depth trends in the mass transfers are not apparent below the saprolite. One sample at 3.5 m depth shows significant loss of Al, Si, and other cations, whereas samples at 3.3 and 3.6 m do not show these losses. All of these samples are above the highest occurrence of macroscopic pyrite grain accumulations in the core. The depletions measured in the sample at 3.5 m may reflect the local effects of acid hydrolysis driven by pyrite oxidation (Brimhall et al., 1985). Additional scatter in $\tau_{j,w}$ below the saprolite is comparable to the variability in the parent material. The saprolite appears therefore to be truly transitional between the organic-rich, weathered soil and the barely altered weathered-rock layers. The bulk density of the saprolite is lower than the weathered rock below it, also suggesting that it has undergone significant mass losses due to weathering.

Comparison with Other Observations

This quantitative analysis of mass losses in the rock and soils is in accord with the mineral variations in the profile (Table 1). We conclude that the weathered appearance arises from oxidation of mafic minerals, which changes the color of the rock without altering its composition or mass. A pair of samples at 6.3 m depth from the inside and outside of an oxidation halo around a fracture supports this view. The pair of samples did not display significant differences in mass transfers ($\tau_{j,w}$) for any element (Fig. 6), other than a slight accumulation of Fe in the oxidized sample. In summary, measurable weathering is limited to the soils and saprolite, where Ca, Na, and Mg have been significantly depleted, and silica has probably been lost, in agreement with the losses in quartz, feldspar, and volcanic glass seen in the thin sections.

Moreover, the data are consistent with the observation that physical disruption, such as bioturbation, is the primary mechanism of regolith production. The positive strain of 2 or more in the soil is roughly an order of mag-

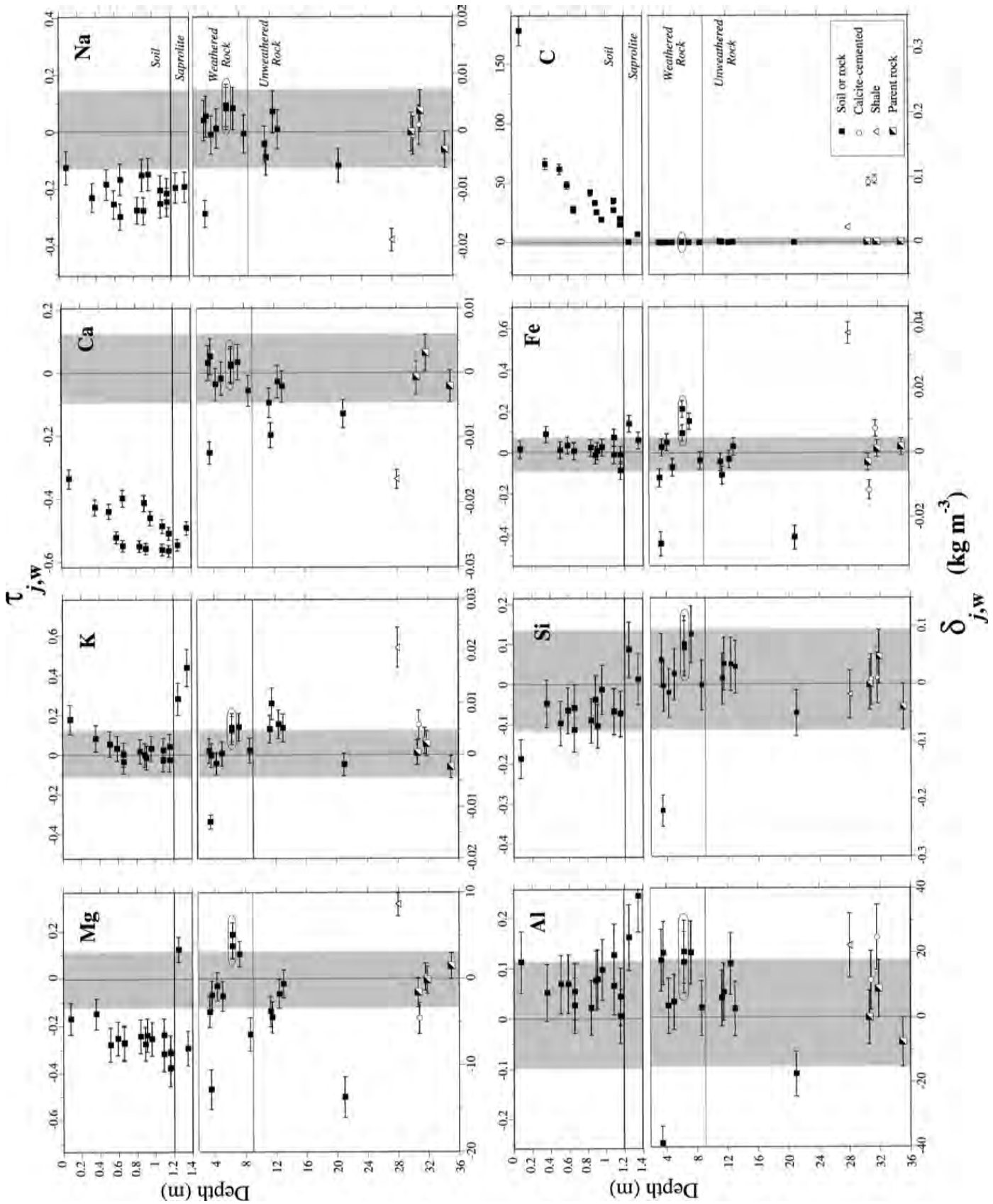
Na
Ca
K
Mg
Si
Fe
C
Al
Soil
Saprolite
Weathered Rock
Unweathered Rock
Soil or rock
Calcite-cemented
Shale
Parent rock
Depth (m)
$\tau_{j,w}$
$\delta_{j,w}$ (kg m^{-3})

Figure 6. Calculated mass gains and losses of major cations, silica, and Al in the weathered rock and soil relative to unweathered parent rock. On each plot, the upper scale expresses changes as a percentage relative to the element mass in the parent rock ($\tau_{j,w}$), whereas the lower scale shows the absolute mass changes per unit volume of parent rock ($\delta_{j,w}$). Error bars represent variations due to the range of parent-material composition on each calculation. Vertical shaded swath shows the effect of this variability on the three parent-rock samples; samples that plot outside of this zone clearly differ in composition from parent material. Circled pair of samples at 6.3 m depth (within the weathered rock) are from the oxidation halo around a fracture and the gray, fresh-looking rock outside the halo. Two calcite-cemented samples are off scale to the right on the Ca plot.

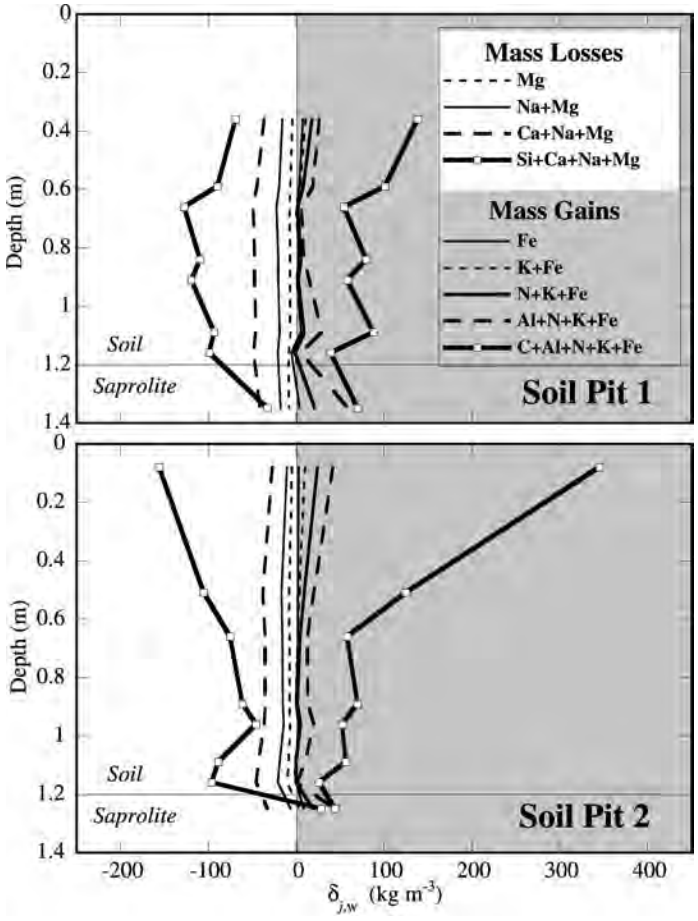

Figure 7. Summary of absolute mass gains and mass losses ($\delta_{j,w}$) in two soil pits in the CB2 catchment. Si and the cations Ca, Na, and Mg are depleted throughout the soils depth; C, N, and Al show mass additions in the soil (shaded side of plot). The mass losses can be summarized as Si > Ca > Na ≥ Mg; mass gains are dominated by C. The deepest sample in each profile is saprolite collected from the bottom of the soil pits. The total mass loss in a column of soil for each pit is reported.

nitude greater than can be explained by addition of organic matter, given a calculated $\delta_{j,w}$ of ~100 kg·m^{-3} for C in the soil and any plausible bulk density for organic matter. Dissolution of silicate minerals produced mass losses in the soil relative to the parent rock of 100–150 kg·m^{-3} (Fig. 7), which corresponds to a porosity increase of 0.04–0.06 for a mineral density of 2600 kg·m^{-3}. At most, then, only ~5% of the soil porosity can be attributed to dissolution of minerals. Most of the porosity and dramatic positive strains in the soil can be credited neither to dissolution of minerals nor to incorporation of organic matter. This finding leads to the conclusion that the strains are derived from purely physical increases in void space, such as would be caused by stress-releasing exfoliation fracturing and by bioturbation- and creep-driven mixing of rock and organic matter.

It is easy to draw the conclusion that physical disruption of the soils is important in their genesis from observations of tree throw, animal burrowing (particularly by mountain beavers, *Aplodontia rufa*), the rapid degradation of landslide scars in the field area, and the very low bulk density of the soil. Exfoliation and raveling on bare bedrock surfaces, and scour during landslides and debris flows, may also be important in the transformation of rock into soil, although these processes are likely to be of secondary importance because they operate over limited areas. Without measuring the rates of these physical processes, however, it is difficult to verify their influence on soil production. The argument just outlined is in accord with our conclusion from the soil water chemistry (Anderson and Dietrich, 2001). The solute-concentration profiles of the soil water should lead to the development of Spodosols within the likely residence times of the soils on these slopes. Spodosols are found on all uplifted marine terraces in the vicinity (Bockheim et al., 1996). The lack of spodic horizons in the CB1 soil we attribute to more frequent disruption of the soil and litter by physical processes than occurs on the low-gradient terraces.

Comparison with Solute Fluxes

To the extent that current weathering processes are reflected in the soil profile, there should be a correspondence between the pattern of solute-mass fluxes and the mass-transfer coefficients calculated from the soil (Stonestrom et al., 1998; White et al., 2002). We therefore compare solute profiles with the solid-phase mass transfers.

Under the steady flow conditions of our sprinkling experiment, soil water solute concentrations are proportional to solute fluxes. How representative are the soil water solute concentrations during steady flow in our sprinkling experiments of typical conditions? Clear-cut logging in 1987 is thought to have had minimal effect on soil water and runoff compositions measured in 1992. Catchment water yield and stream chemistry generally return to baseline within five years (Jewett et al., 1995; Swank et al., 2001). In Oregon Coast Range soils, nutrient concentrations do not vary between 5 yr stands and old growth (Entry and Emmingham, 1995). Also, runoff chemistry varies <20% per tenfold variation in discharge over a range of four orders of

magnitude. Runoff composition variations are attributed to changes in flow paths and residence time of water in bedrock under different hydrologic conditions (Anderson et al., 1997a). Soil water solute concentrations were quite stable throughout experiment 3 (Anderson and Dietrich, 2001). In Figure 8, we show that soil water during experiment 3 is comparable with soil water from the peak of a winter storm (February 20, 1992). The storm had a peak rainfall intensity of 15 $mm \cdot h^{-1}$, an order of magnitude greater than experiment 3, and produced instantaneous discharge 10 times greater than experiment 3 (Anderson et al., 1997b). Because of the remarkable consistency in soil water during these different hydrologic conditions and different times in the growing season, we feel that the steady flow condition is representative of typical solute flux conditions.

The mass balance of any constituent in a vertical column of soil during steady solute flux conditions is

$$\frac{\partial M}{\partial t} = -\nabla \cdot Q_d = -\frac{\partial Q_x}{\partial x} - \frac{\partial Q_y}{\partial y} - \frac{\partial Q_z}{\partial z}, \quad (5)$$

where M is the mass and Q_d is the dissolved mass flux per unit area of that constituent. Noting that the solute fluxes may be written $Q_i = U_i C$, where U_i is the water velocity in the i direction and C is the solute concentration, and given the specific conditions of steady vertical flow achieved in experiment 3, equation 5 simplifies to

$$\frac{\partial M}{\partial t} = -U_z \frac{\partial C}{\partial z}. \quad (6)$$

Because the vadose-zone water during experiment 3 moved vertically at a constant velocity, U_z, within the soil (Torres et al., 1998), interpretation of mass change in the soil resulting from the solute flux is straightforward. Regions of increasing concentration with depth undergo net mass removal, whereas regions of negative solute concentration gradients accumulate the solute in question.

The increasing Si concentrations in soil waters with depth (Fig. 8) show that silica is lost in solution throughout the soil profile owing to chemical weathering. Our analysis of the solid phase suggest silica losses throughout the soil profile (Fig. 6). If we take the soil silica data at face value, a stance in accord with both the thin-section analysis and the fact that all soil samples have negative $\delta_{Si,w}$ values, we find that the greatest solid-phase mass losses in the soil are from silica and these are relatively uniformly distributed through the soil profile (Fig. 7). The humped solute profiles of Al, Fe, and K should result in translocation and accumulation of these species within the soil; instead, all show small mass gains (accumulation) in the solid phase throughout the soil pits, with no evidence of a zone of removal. Ca and Na display relatively uniform solute concentrations with depth, after a steep rise in the top 0.2 m of the soil. This circumstance should yield mass losses of these elements concentrated near the soil surface, yet both show uniform mass losses throughout the soil solid phase. Mg solute concentrations are lowest of all the cations, which is reflected in Mg mass losses in the solid phase being lower than Na and Ca. In general, the solute-concentration profiles suggest that mass losses should be concentrated near the soil surface, rather than be uniform with depth.

Some of the discrepancies between the solute behavior and the mass changes in the solid phase may arise from the fact that solutes and soils were not sampled within the same profile. A more significant difference between the two records, however, is that the solute profiles show one moment in time, whereas the solid-phase profiles show the accumulated effects of weathering over significant periods of time (several thousand years). Mechanical mixing will tend to obliterate vertical patterns of mass change through homogenization. Changes in solute concentrations of K, Al, Ca, and Na are greatest in the top 0.5–0.6 m of the lysimeter profiles (Fig. 8), and therefore, gradients in the solid-phase mass gains and losses of these elements should be found within this depth range in the soil pits. The relative uniformity of the mass losses of Ca and Na through the soil profiles and the absence of a zone of removal of Al and K in the solid phase (Fig. 6) suggest that, over time, bioturbation homogenizes the soil to at least these depths. Si concentrations in the soil solution increase steadily downward through the lysimeter profiles, which should result in uniform mass losses of silica in the soil profiles, a pattern that cannot be disrupted by bioturbation. Except for the litter sample at the top of soil pit 2, and the saprolite samples at the bottoms of both soil pits, mass losses of silica are relatively uniform in the soil pits, in agreement with the prediction from solute profiles. Thus, the soil water chemistry, the soil development, and the elemental chemistry of the soils all point to physical processes being very important in the genesis and subsequent evolution of the soils in the CB1 catchment.

RATE OF MASS LOSS IN SOIL VERSUS ROCK

From the analysis of mass losses in the solid phase, it is easy to get the impression that all weathering takes place within the soil. This interpretation is at odds, however, with a conclusion from experiment 3 that solute fluxes from the site were derived roughly equally from the soil and from the bedrock (Anderson and Dietrich, 2001). The total solute flux through the soil, calculated from the soil water TDS (total dissolved solids) concentrations and vadose-zone water flux, equaled half of the total solute flux out of the catchment during experiment 3. Soil water travels through the bedrock before emerging at the channel head, and therefore the additional solute in the runoff must be derived from bedrock. Because the soil thickness is less than the weathered-rock thickness, this observation suggests that weathering in the soil is more intense than in the bedrock.

To explore this proposition, we computed the rate of mass loss per unit volume of parent rock measured over the time scale for development of the weathered profile. We first established the residence time for parcels of rock in the weathered rock and of soil layers in the weathered profile. We used several methods to address the determination of residence time for the soil and a single method—based on uplift rates—for the weathered rock. Residence time in both layers must be set by the uplift rate and layer thickness, assuming that these layers have constant thickness through time. This condition is equivalent to an assumption of a landscape in dynamic equilibrium (Hack, 1960; Pavich, 1986); that is, maintenance of landforms and the weathering profiles on them, while erosion rates exactly match uplift rates.

Residence Time from Uplift Rates

Because the weathered-rock profile ranges from 3 to 8 m thick in the CB1 catchment, 5 $\pm$ 1 m is a reasonable average thickness. The average soil depth in the CB1 catchment is 0.70 m. However, because the bulk density of the soil is significantly lower than that of rock, the equivalent thickness of rock represented by the soil, or the ''effective thickness'' of the soil, is just 0.23 m. For local uplift rates, we used 0.1 $\pm$ 0.07 $mm \cdot yr^{-1}$, which is centered on the most likely uplift rate for the region (H. Kelsey, 1994, personal commun.), but also

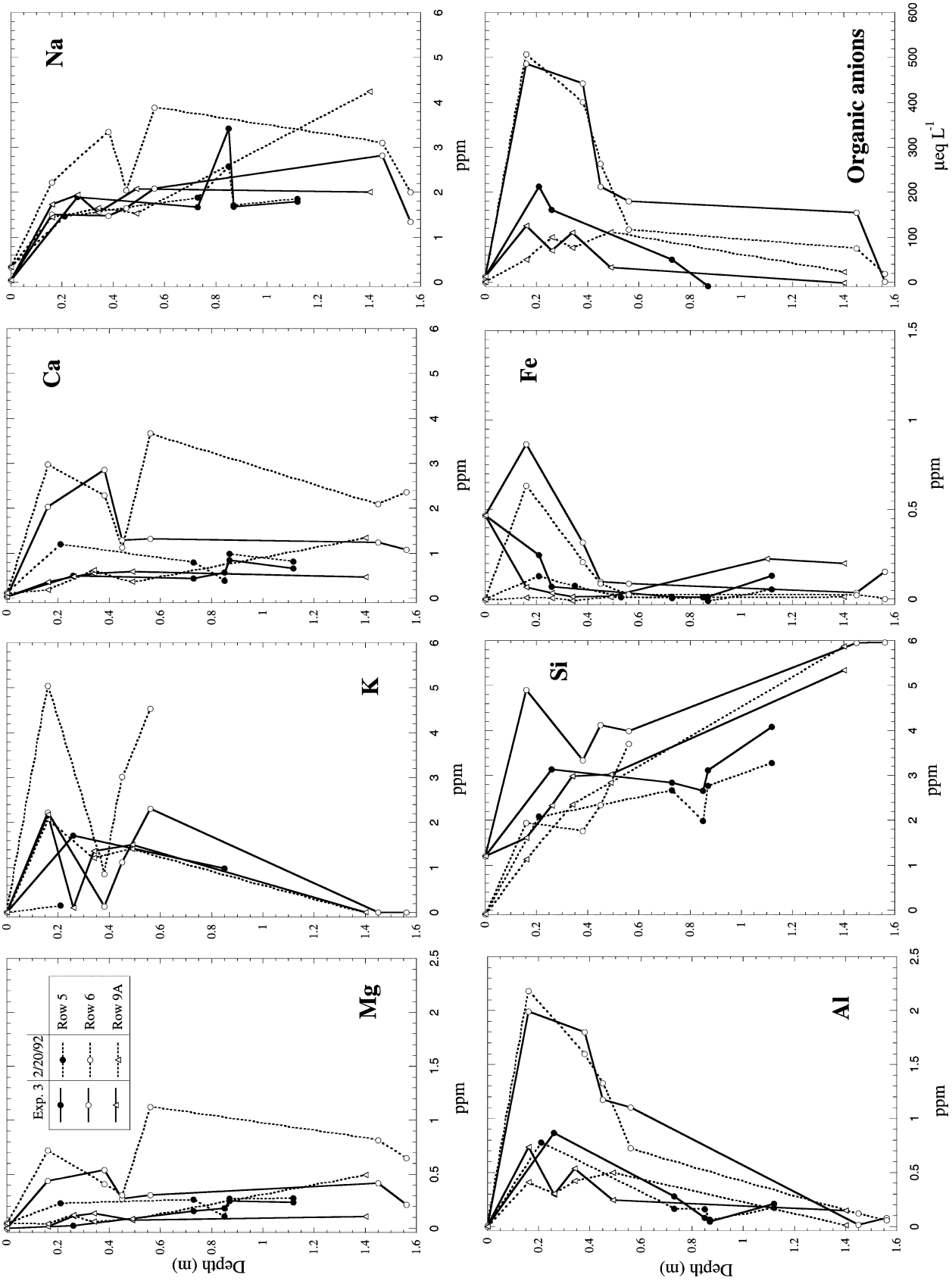

Figure 8. Soil water concentration profiles on May 31, 1992, during the steady flow conditions of sprinkling experiment 3 (solid lines) and on February 20, 1992, during the largest storm of the winter (dotted lines). Lysimeter nests numbered according to the access row on which they are located (see Fig. 4).

TABLE 2. RESIDENCE TIME ESTIMATES

Layer	Thickness (m)	Effective thickness (m)	Residence times (k.y.)			
			From uplift rates	From $\delta_{j,w}$ and solute flux	^{14}C date	Reneau and Dietrich (1991)
Soil	0.70	0.23	2.3 ± 1.8	3.5 ± 1.4	4.07 ± 0.09	5–6
Weathered rock, including saprolite	5	5	50 ± 36			

encompasses most of the likely range. For this uplift rate, the residence time in the weathered-rock layers is 50 ± 36 k.y., and the residence time in the soil is 2.3 ± 1.8 k.y. (Table 2). Much of the error comes from the wide range of possible uplift rates, which affect both residence times the same way. A parcel of rock spends ~20 times longer traversing the weathered-rock layers than passing through the soil.

Residence Time from Solute Fluxes

An alternative method is to use solute fluxes and our measurements of mass loss in the solid phase of the soil. Several others have found a close correspondence between modern solute fluxes and long-term weathering rates determined from calculated soil mass losses (Stonestrom et al., 1998; White et al., 1998). The residence time for material in the weathered profile, t_w, is calculated from the sum of mass losses in the soil $\Sigma(\delta_{j,w})$ integrated over the soil depth, the mean annual runoff, Q_{annual}, and the average sum of dissolved concentrations of the elements considered, $\Sigma_j \bar{C}_j$:

$$t_w = \frac{\int_0^{H_s} \sum_j (\delta_{j,w})\, dz}{Q_{annual} \sum_j \bar{C}_j}, \qquad (7)$$

where H_s is the soil depth. The numerator is the total mass loss from the soil solid phase, and the denominator is the rate of mass loss in solution.

The numerator of equation 7, computed as the product of the average $\delta_{j,w}$ values for Si, Ca, Na, and Mg from the soil pits (= 94.5 ± 27.7 kg·m^{-3}) and the average soil thickness, is 66.2 ± 19.4 kg·m^{-2}. For the denominator, we used the mean annual runoff from the CB1 catchment of 1.6–1.8 m·yr^{-1} (Anderson, 1995), and the average dissolved cations plus silica concentration in the soil during steady runoff in experiment 3 of 11.0 ± 3.0 ppm (Anderson and Dietrich, 2001). The soil residence time calculated from equation 7 is 3.5 ± 1.4 k.y.

Other Measures

We have two additional independent age estimates for the soil. A ^{14}C age of 4070 ± 90 yr B.P. (Center for Accelerator Mass Spectrometry, Lawrence Livermore National Laboratory) on charcoal from the base of soil pit 1 in the CB2 catchment is in good agreement with the values in Table 2. Reneau and Dietrich (1991) calculated residence times of 5–6 k.y. for colluvium in the southern Oregon Coast Range, based on ^{14}C age dates of colluvial fills.

Depth of Significant Mass Loss in the Weathered Rock

The similarities between the residence times computed for the soil from the approaches just outlined supports the idea that the local landscape is in dynamic equilibrium. This statement means that the soil does not change in thickness with time and that regolith production and erosion both occur at the same rate. It is likely that this dynamic equilibrium extends to the weathered-rock layers as well. A consequence of the combination of dynamic equilibrium and equal partitioning of solute fluxes from the soil and the bedrock is that we should expect to see equivalent solid-phase mass losses in the soil and bedrock despite the disparity in residence times within these layers. We make this prediction because in steady state, the residence time, t_r, and thickness of layers, H, are related through the uplift rate, $u = H/t_r$. Material in the thinner soil layer thus has a shorter residence time than in the thicker weathered rock in proportion to the uplift rate. We can calculate the average change in density, $\Delta\bar{\rho}$, in a layer due to mass loss in solution as

$$\Delta\bar{\rho} = -\frac{Q_w(C - C_0)}{u}, \qquad (8)$$

where Q_w is the water flux (in m/yr), and (C—C_0) is the change in solute concentration as water flows through the layer. Because the net solute fluxes from the soil and bedrock layers at CB1 are roughly identical (Anderson and Dietrich, 2001), the change in density is the same within the layers. This circumstance should be manifested by similar integrated mass losses in the soil layer and the weathered-rock layer.

From the measured annual water flux of 1.6–1.8 m/yr, average bedrock-derived cations plus silica concentration in the runoff of 9.4 ± 3.0 ppm (Anderson and Dietrich, 2001), and uplift rate of 0.10 ± 0.07 mm/yr, we obtain an average change in density within the weathered bedrock layer of 160 ± 123 kg/m^3. A change in density of this magnitude is certainly measurable; therefore, the lack of observable density variation within the bedrock core samples does not stem from too small a signature. The average bulk density of all the samples from the core is 2270 ± 60 kg/m^3, whereas bulk densities of two saprolite samples from the soil pits are 1150 and 1850 kg/m^3 (Fig. 3). These saprolite samples have undergone density losses of 1120 and 420 kg/m^3, respectively. That the saprolite samples display mass losses much greater than the average density change we have just computed for the weathered-rock layer is reasonable for samples from the top of a profile in which the degree of weathering declines with depth.

Our sampling was not sufficiently dense at the top of the weathered rock to allow us to identify the thickness of the weathered-rock layer that has undergone significant mass losses or to define how these mass losses vary with depth. To put limits on the thickness of this significantly weathered rock layer, we appeal to our observation that integrated mass losses in the weathered rock must equal those of the soil. The integrated mass losses in the bedrock are equal to the average density change multiplied by an appropriate depth $(\Delta\bar{\rho})H$. This can be equated to the integrated mass loss in the soil:

$$(\Delta\bar{\rho}_R)H_R = \int_0^{H_s} \sum_j (\delta_{j,w})\, dz, \qquad (9)$$

where the left side shows the mass losses in the rock and the right side shows the mass losses in the soil. We have already found that the right side of equation 9 is 66.2 ± 19.4 kg·m^{-2} and that $\Delta\bar{\rho}$ is 160 ± 123 kg·m^{-3}. Therefore, the representative thickness, H_R, for the weathered-rock layer is 0.41 ± 0.34 m.

Constraints on the distribution of mass losses in the weathered rock are depicted in Figure 9. The total mass loss in the weathered-rock layer is equal to the area of the box in Figure

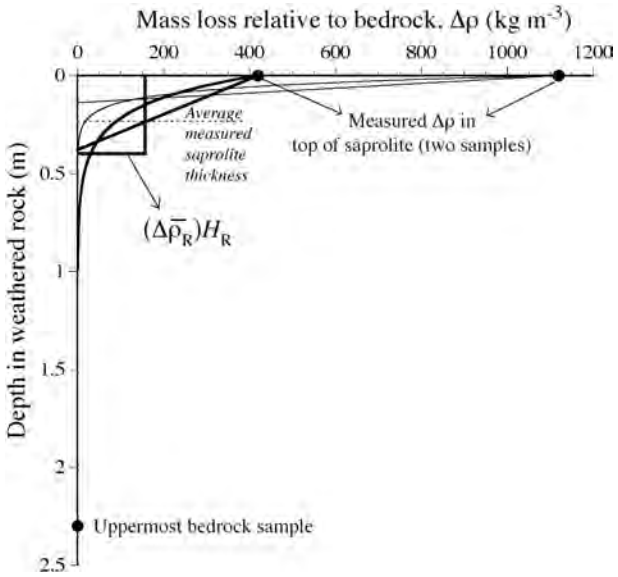

Figure 9. Plausible models of vertical distribution of mass losses in the weathered rock. Box shows integral constraint on mass losses determined from $(\Delta\bar{\rho}_R)H_R$. Average measured saprolite thickness (dashed line) falls within this layer of significant mass loss. Points at 0 depth show measured density differences in saprolite samples collected at the base of soil pits (the top of the weathered rock); point at 2.3 m depth shows the uppermost core sample. Pairs of curves (one pair light, one pair bold) show linear and exponential distributions of Δρ that fit the integral constraint for each of the two saprolite measurements. In all cases, the depth of significant mass losses due to weathering is confined to a layer <1 m thick (generally <0.4 m thick).

9 whose sides are $\Delta\bar{\rho} = 160$ kg·m^{-3} and $H_R = 0.4$ m. Measurements of Δρ in the two saprolite samples and of $\Delta\rho = 0$ for the uppermost sample of the bedrock core are shown as points. By using the saprolite Δρ values and the integral constraint on total mass loss, we can construct the Δρ profiles for cases of linear and exponential decline in mass loss with depth. In all four cases, significant mass losses are confined to the top 1 m of the weathered rock, and most likely to the top 0.4 m, well above our uppermost core sample at 2.3 m into the weathered rock. These profiles compare well with an average saprolite thickness in our borings (in the 36 cores where we encountered it) of 0.23 ± 0.26 m. Saprolite, however, was not found throughout the catchment. This analysis yields average mass loss in the weathered rock throughout the catchment. The good agreement between saprolite thickness and average depth of significant mass loss in the catchment implies that these mass losses are probably not confined to just the saprolite layer itself, but may also be found in the uppermost weathered rock where saprolite is missing. That the degree of weathering in the top of the bedrock, as represented by the bulk density loss, is so variable suggests that conversion of rock to soil is driven by stochastic events of relatively small length scale, in agreement with the assessment of Heimsath et al. (2001b).

We can now address the rate of mass loss in the soil versus the bedrock. The rate of mass loss per unit volume of rock, or I_w, is $\Delta M/(V\Delta t)$, where ΔM is the integrated mass loss, V is volume, and Δt is the time over which the mass loss occurs. If we consider mass losses in a column of rock or soil, and therefore replace volume with thickness (i.e., volume per unit area), and note that residence time is the thickness divided by the uplift rate, the rate of mass loss in a layer of thickness H can be expressed as

$$I_w = \frac{\Delta M}{H(H/u)}. \quad (10)$$

Because ΔM for the soil equals ΔM in the weathered rock in CB1, the ratio of rate of mass loss in the soil to rate of mass loss in the weathered rock reduces to

$$\frac{I_S}{I_R} = \frac{H_R{}^2}{H_S{}^2}, \quad (11)$$

where subscripts S and R refer to soil and weathered rock, respectively. Dynamic equilibrium leads to the squared dependence on the layer thickness, as the residence time within a layer depends on thickness.

The ratio of rate of mass loss in the soil to the weathered rock in the CB1 catchment therefore depends on the thickness of the layer that has undergone significant mass loss in the weathered rock. If the calculated 0.4 m average depth of mass loss is appropriate for the rock, and the soil is 0.23 m in depth (rock equivalent), then this ratio is 3. For the profiles shown in Figure 9, the ratio ranges from 0.21 to 11. The smaller ratio, which implies much greater rate of mass loss in the rock than in the soil, is for the case that yields the thinnest zone of weathering in the rock, whereas the larger ratio is for a weathered-rock layer of 1 m thickness. Using the average saprolite thickness of 0.23 ± 0.26 m yields a ratio of 1, meaning that the rate of mass loss within the bedrock is the same as that in the soil.

Although our data on rate of mass loss in the soil versus the rock is equivocal, we think that a greater rate of mass loss in the soil is the most likely scenario. The degree of weathering at the top of the weathered-rock profile clearly varies significantly throughout the catchment. The samples of rock collected at the base of our two soil pits differ in Δρ by a factor of two. Saprolite is absent in parts of the catchment and up to 1 m thick elsewhere. Given this variability, our computed average depth of significant mass loss of 0.4 m in the bedrock provides the best measure of the typical weathered-rock profile. This thickness implies that rate of mass loss in the soil is approximately three times greater than in the rock.

There are a number of reasons that weathering may be more intense within the soil than the rock. First, the effects of vegetation on weathering will be strongest in the soil. In general, vegetation affects chemical-weathering rates by producing weathering agents, cycling cations, and altering soil hydrology (Kelly et al., 1998). Organic acids, which mediate silicate weathering through chelation of cations and metals, peak in concentration in the upper 0.5 m of the CB1 soil (Fig. 8). Second, bypassing flow routes (root holes, soil fractures) are not significant in the CB1 soils, whereas fracture flow is important in the bedrock. Thus, more water passes through the soil matrix than through the bedrock matrix, giving greater contact with mineral surfaces in the soil. Chemical-weathering rates depend on both water velocity (which sets contact time) and water flux. At CB1, the maximum in contact time and water flux appears to be met in the soil. We found that water-flow rates

TABLE 3. LONG-TERM SILICA FLUXES

Location	Reference	Mean annual precipitation (m)	Mean annual temperature (°C)	Soil age (ka)	Si flux (t km^{-2} yr^{-1})
CB1	This study	1.6–1.8	9*	3.5 ± 2.5	10.7 ± 7.1
Rio Icacos, Puerto Rico	White et al. (1998); Stonestrom et al. (1998)	4.2	22	200	14.9
Panola, Georgia	Stonestrom et al. (1998)	1.2	16	350	4.8
Riverbank soil, California	Stonestrom et al. (1998)	0.3	16	250	2.2
Strawberry Rock soil, California	Chadwick et al. (1990)	1–1.5	12	240	2.1

*Data from National Climate Data Center, for North Bend Municipal Airport, assuming a 6 °C/km lapse rate.

through the soil vadose zone were controlled by rainfall rates (Anderson et al., 1997b; Torres et al., 1998), commonly ~1 mm·h^{-1}, or ~10^{-6} m·s^{-1}. These rates are comparable to the few measurements of saturated hydraulic conductivity in near-surface weathered-bedrock matrix of 10^{-5} to 10^{-7} m·s^{-1} (Montgomery et al., 1997). A significant fraction of the water flow through the bedrock, however, occurs through fractures, where high velocities (~10^{-3} m·s^{-1}) and little contact with mineral surfaces both work to limit solute acquisition. Thus, the water flux through the rock matrix is less than in the soil because some flow bypasses the rock in fractures or along the soil/rock interface. We found no evidence for bypass flow in the soil.

DISCUSSION

Weathering of the rock starts with opening of fractures. As rock moves up through the profile, the number of fractures increases (Fig. 2). These provide avenues for water flow through the rock, but the passage of that water is relatively rapid. With time, the number of fractures increases and oxidation halos grow, eventually coalescing to form a pervasively oxidized rock layer. In the upper 0.4 m of this layer (on average), weathering produces significant mass losses; consequently, changes in bulk density are found. Where physically undisturbed, chemical degradation continues to the point of loss of mechanical strength, and saprolite forms. Although we have not tried to measure it, it seems likely that matrix hydraulic conductivity must increase upward through the pervasively oxidized rock and saprolite layers, as weathering produces porosity. Increasing water flow through the rock matrix as it weathers provides a positive feedback on the chemical-weathering rate within the rock. Finally, material is transformed from rock into soil by physical or physical and biological processes that tear up and transport rock fragments. These regolith-forming processes feed material into the final stage of weathering within the profile. In the soil, water flows readily through the matrix. The presence of organic acids, high P_{CO_2}, and oxygen all contribute to enhancing chemical-weathering rates. Chemical weathering is most intense within the soil layer, but it is also significant within the rock. Water flow is a key to the rates of chemical processes within both rock and soil, and the reason that half of the solute from the CB1 catchment derives from the rock is that nearly all water flows through the bedrock in its passage through the catchment.

Throughout the weathered profile, chemical weathering processes operate in tandem with physical processes except during two physically driven transformations. These are the formation of regolith (soil) from the underlying rock and the transport of soil out of the catchment. These two key events check further chemical evolution of the rock (in the first case) or of the soil (in the second). Because these events are physically driven, physical processes set the time scale—and hence the degree of development of the weathered profile—and chemical weathering plays a secondary role.

Although physical processes control weathered-profile development and regolith formation, the degree of chemical weathering that takes place within this framework is remarkable. Within the 1–10 k.y. residence time in the saprolite and soil, 25%–50% of cations and perhaps 10% of the silica in the rock are removed. By comparison, Chadwick et al. (1990) measured Si losses of 29% and Na losses of 57% in a 240 ka soil in northern California. If the residence time of material in the CB1 soil were increased, it seems likely that aluminous clay phases would accumulate and change the soil's hydraulic properties. For example, the soil studied by Chadwick et al. (1990) contained 30% secondary clay. The effect of clay formation on soil water movement is one source of the difference in rate of mass loss between these sites. Another difference is the lack of topographic gradient driving erosion and refreshing material in the soils that Chadwick et al. (1990) studied.

The long-term silica flux from the CB1 catchment soils—computed from the measured average Si loss in the soil ($\delta_{Si,w}$ = 54.1 ± 28.3 kg·m^{-3}), the average soil thickness, and the average residence time for material in the soil of 3.5 ± 1.4 k.y. (Table 2)—is 10.7 ± 7.1 t·km^{-2}·yr^{-1}. This value falls above the long-term silica fluxes calculated in several other catchments on the basis of similar analyses of soil and runoff chemistry (Table 3). Among these, only the example from the tropical Rio Icacos soil yields a greater silica flux than does the CB1 soil. Extremely high rainfall and temperature may account for the high weathering rates from the Rio Icacos soil. Although we cannot rule out weathering of volcanic glass as the source of high silica fluxes from CB1, the most striking difference between the remaining sites and the CB1 catchment is the age of the soil. This difference suggests that the ongoing rejuvenation of CB1 soils by physical regolith-production processes sustains higher chemical-weathering rates than would be reached in a more stable environment. Riebe et al. (2001) found in granitic Sierra Nevada catchments that silica fluxes were greatest in the areas undergoing the most rapid physical denudation. The CB1 silica flux of 10.7 ± 7.1 t·km^{-2}·yr^{-1} and erosion rate of 110–180 t·km^{-2}·yr^{-1} (Reneau and Dietrich, 1991) are comparable to the 2–8 t·km^{-2}·yr^{-1} range that Riebe et al. (2001) reported for Sierran catchments with total erosion rates of ~100 t·km^{-2}·yr^{-1}.

The connection between uplift and silicate chemical weathering appears to be as follows. At very high uplift or physical-denudation rates, soil may be very thin or absent. This circumstance will yield low, but nonnegligible chemical denudation rates associated with weathering within the bedrock. Fracture flow, the likely dominant hydrologic pathway in bedrock, limits both the surface area of minerals in contact with water and the contact time. At lower uplift and physical-denudation rates, the landscape may be thinly soil mantled, and chemical weathering will take place in both the soil and the rock. This situation exists at CB1, where half of all weathering takes place within the rock, and silica fluxes are quite high. At low or negligible uplift and physical-denudation rates, soils will thicken,

and we think that chemical-weathering rates will be reduced. At this end of the spectrum, low physical-process rates mean that soils can develop into mature profiles. Development of clay may impede water flow through the soil, whereas thickening the soil may lead to chemical saturation control on chemical-weathering rates (e.g., White et al., 2001). Together, these effects suggest that silicate chemical-weathering rates will be greatest at some intermediate uplift or physical-denudation rate, where physical processes are rapid enough to continually add fresh rock into the weathering profile, yet low enough to permit development of a soil.

CONCLUSIONS

The weathered profile in this steep, actively eroding headwater basin consists of a loose, poorly developed ~0.7 m deep soil overlying 3–8 m of weathered rock. The total mass lost by chemical weathering is as great from the rock as from the soil. Because the thickness of the weathering layer is greater in the rock than in the soil (normalized to equivalent density), the rate of mass loss is greater in the soil than in the rock. Soils are important sites of chemical weathering, because the combination of hydrology and biology that they support generally enhances solute-production rates. Although weathering within bedrock is often ignored (e.g., Riebe et al., 2001), this work demonstrates that bedrock can also be a significant site of chemical weathering.

The silica flux of 10.7 ± 7.1 $t \cdot km^{-2} \cdot yr^{-1}$ from the CB1 catchment is higher than that from other catchments with considerably older weathering profiles (Table 3) and is comparable to silica fluxes from catchments with similar physical-denudation rates (Riebe et al., 2001). We infer that physical processes enhance chemical-weathering rates by rejuvenating and refreshing material within the soil ''reactor.'' The hydrology of a young, bioturbated soil is also conducive to high solute fluxes because of the lack of impeding horizons. These observations suggest that chemical-weathering rates from catchments depend on physical-denudation rates and therefore on uplift rates. However, we infer that the relationship between chemical weathering and uplift rates is not likely to be monotonic. When uplift rates are high enough that the landscape becomes bedrock dominated, hydrologic contact with mineral surfaces diminishes (fracture flow dominates), and enhancement of weathering by biotic processes declines. Both of these effects will tend to lower the chemical denudation rate. This result parallels our arguments that rate of mass loss within the bedrock at CB1 is lower than within the soil. The implication is that areas undergoing the highest uplift rates will not produce the highest silicate-weathering rates. Instead, silicate-weathering rates will be maximized in actively eroding, soil-mantled landscapes.

ACKNOWLEDGMENTS

We thank Tim Teague, C. Lewis, and L. Abbott for assistance with the laboratory work and O. Chadwick for discussions about the mass-balance model. We appreciated thoughtful reviews by S. Brantley, R. Stallard, and associate editor J. Hanor. This work was supported by a National Aeronautics and Space Administration global change graduate fellowship (NGT30083), the National Science Foundation (EAR8417467), the U.S. Geological Survey Water Resources Division (14080001G12111), and the Weyerhauser Company. CSIDE (Center for Study of Imaging and Dynamics of the Earth) contribution number 438.

REFERENCES CITED

Adams, J., 1984, Active deformation of the Pacific Northwest continental margin: Tectonics, v. 3, p. 449–472.

Ahnert, F., 1967, The role of the equilibrium concept in the interpretation of landforms of fluvial erosion and deposition, *in* Macar, P., ed., L'Evolution des Versants: Les Congress et Colloques de l'Université de Liege, v. 40, p. 23–41.

Anderson, R.S., 1999, Near-surface thermal profiles in alpine bedrock: Implications for the frost weathering of rock: Arctic and Alpine Research, v. 30, p. 362–372.

Anderson, R.S., and Humphrey, N.F., 1989, Interaction of weathering and transport processes in the evolution of arid landscapes, *in* Cross, T., Quantitative Dynamic Stratigraphy: Englewood Cliffs, New Jersey, Prentice-Hall, p. 349–361.

Anderson, S.P., 1995, Flow paths, solute sources, weathering, and denudation rates: The chemical geomorphology of a small catchment [Ph.D. thesis]: Berkeley, University of California, 380 p.

Anderson, S.P., and Dietrich, W.E., 2001, Chemical weathering and runoff chemistry in a steep headwater catchment: Hydrological Processes, v. 15, p. 1791–1815.

Anderson, S.P., Dietrich, W.E., Torres, R., Montgomery, D.R., and Loague, K., 1997a, Concentration-discharge relationships in a steep, unchanneled catchment: Water Resources Research, v. 33, p. 211–225.

Anderson, S.P., Dietrich, W.E., Montgomery, D.R., Torres, R., Conrad, M.E., and Loague, K., 1997b, Subsurface flow paths in a steep unchanneled catchment: Water Resources Research, v. 33, p. 2637–2653.

Baldwin, E.M., 1974, Eocene stratigraphy of southwestern Oregon: Oregon Department of Geology and Mineral Industries Bulletin, no. 83, 38 p.

Baldwin, E.M., 1975, Revision of the Eocene stratigraphy of southwestern Oregon, *in* Weaver, D.W., Hornaday, G.R., and Tipton, A., eds., Paleogene symposium and selected technical papers—Conference on future energy horizons of the Pacific Coast: Long Beach, California, American Association of Petroleum Geologists, p. 49–64.

Berner, R.A., 1990, Atmospheric carbon dioxide levels over Phanerozoic time: Science, v. 249, p. 1382–1386.

Bockheim, J.G., Marshall, J.G., and Kelsey, H.M., 1996, Soil-forming processes and rates on uplifted marine terraces in southwestern Oregon, USA: Geoderma, v. 73, p. 39–62.

Brimhall, G.H., Alpers, C.N., and Cunningham, A.B., 1985, Analysis of supergene ore-forming processes and ground water solute transport using mass balance principles: Economic Geology, v. 80, p. 1227–1256.

Brimhall, G.H., and Dietrich, W.E., 1987, Constitutive mass balance relations between chemical composition, volume, density, porosity, and strain in metasomatic hydrochemical systems: Results on weathering and pedogenesis: Geochimica et Cosmochimica Acta, v. 51, p. 567–587.

Brimhall, G.H., Lewis, C.J., Ford, C., Bratt, J., Taylor, G., and Warin, O., 1991, Quantitative geochemical approach to pedogenesis: Importance of parent material reduction, volumetric expansion, and eolian influx in lateritization: Geoderma, v. 51, p. 51–91.

Brimhall, G.H., Chadwick, O.A., Lewis, C.J., Compston, W., Williams, I.S., Danti, K.J., Dietrich, W.E., Power, M.E., Hendricks, D., and Bratt, J., 1992, Deformational mass transport and invasive processes in soil evolution: Science, v. 255, p. 695–702.

Carson, M.A., and Kirkby, M.J., 1972, Hillslope form and process: Cambridge, UK, Cambridge University Press, 475 p.

Chadwick, O.A., Brimhall, G.H., Jr., and Hendricks, D.M., 1990, From a black to a gray box—A mass balance interpretation of pedogenesis: Geomorphology, v. 3, p. 369–390.

Dahlgren, R.A., and Ugolini, F.C., 1989, Aluminum fractionation of soil solutions from unperturbed and tephra-treated Spodosols, Cascade Range, Washington, USA: Soil Science Society of America Journal, v. 53, p. 559–566.

Dietrich, W.E., Reneau, S.L., and Wilson, C.J., 1986, Hollows, colluvium, and landslides in soil-mantled landscapes, *in* Abrahams, A.D., ed., Hillslope processes: Boston, Allen and Unwin, p. 361–388.

Dott, R.H., Jr., 1966, Eocene deltaic sedimentation at Coos Bay, Oregon: Journal of Geology, v. 74, p. 373–420.

England, P., and Molnar, P., 1990, Surface uplift, uplift of rocks, and exhumation of rocks: Geology, v. 18, p. 1173–1177.

Entry, J.A., and Emmingham, W.H., 1995, Influence of forest age on nutrient availability and storage in coniferous soils of the Oregon Coast Range: Canadian Journal of Forest Research, v. 25, p. 114–120.

Gaillardet, J., Dupré, B., Louvat, P., and Allègre, C.J., 1999a, Global silicate weathering and CO_2 consumption rates deduced from the chemistry of large rivers: Chemical Geology, v. 159, p. 3–30.

Gaillardet, J., Dupré, B., and Allègre, C.J., 1999b, Geochemistry of large river suspended sediments: Silicate weathering or recycling tracer? Geochimica et Cosmochimica Acta, v. 63, p. 4037–4051.

Gilbert, G.K., 1877, Report on the geology of the Henry Mountains (Utah): Washington, D.C., U.S. Geographical and Geological Survey, Publication of the Powell Survey, Government Printing Office, 160 p.

Haagen, J.T., 1989, Soil survey of Coos County, Oregon: U.S. Department of Agriculture, Soil Conservation Service, 269 p.

Hack, J.T., 1960, Interpretation of erosional topography in humid temperate regions: American Journal of Science, v. 258-A, p. 80–97.

Heimsath, A.M., Dietrich, W.E., Nishiizumi, K., and Finkel, R.C., 1997, The soil production function and landscape equilibrium: Nature, v. 388, p. 358–361.

Heimsath, A.M., Dietrich, W.E., Nishiizumi, K., and Finkel, R.C., 1999, Cosmogenic nuclides, topography, and the spatial variation of soil depth: Geomorphology, v. 27, p. 151–172.

Heimsath, A.M., Chappell, J., Dietrich, W.E., Nishiizumi, K., and Finkel, R.C., 2000, Soil production on a retreating escarpment in southeastern Australia: Geology, v. 28, p. 787–790.

Heimsath, A.M., Chappell, J., Dietrich, W.E., Nishiizumi, K., and Finkel, R.C., 2001a, Late Quaternary erosion in southeastern Australia: A field example using cosmogenic nuclides: Quaternary International, v. 83–85, p. 169–185.

Heimsath, A.M., Dietrich, W.E., Nishiizumi, K., and Finkel, R.C., 2001b, Stochastic processes of soil production and transport: Erosion rates, topographic variation and cosmogenic nuclides in the Oregon Coast Range: Earth Surface Processes and Landforms, v. 26, p. 531–552.

Holland, H.D., 1978, The chemistry of the atmosphere and oceans: New York, John Wiley and Sons, 351 p.

Jewett, K., Daugharty, D., Krause, H.H., and Arp, P.A., 1995, Watershed responses to clear-cutting: Effects on soil solutions and stream water discharge in central New Brunswick: Canadian Journal of Soil Science, v. 75, p. 475–490.

Kelly, E.F., Chadwick, O.A., and Hilinski, T.E., 1998, The effect of plants on mineral weathering: Biogeochemistry, v. 42, p. 21–53.

Kelsey, H.M., Engebretson, D.C., Mitchell, C.E., and Ticknor, R.L., 1994, Topographic form of the Coast Ranges of the Cascadia margin in relation to coastal uplift rates and plate subduction: Journal of Geophysical Research, v. 99, p. 12245–12255.

Kelsey, H.M., Ticknor, R.L., Bockheim, J.G., Mitchell, C.E., 1996, Quaternary upper plate deformation in coastal Oregon: Geology Society of America Bulletin, v. 108, p. 843–860.

Lovell, J.P.B., 1969, Tyee Formation: Undeformed turbidites and their lateral equivalents: Mineralogy and paleogeography: Geological Society of America Bulletin, v. 80, p. 9–22.

MacDonald, L.H., 1988, An inexpensive, portable system for drilling into subsurface layers: Soil Science Society of America Journal, v. 52, p. 1817–1819.

Montgomery, D.R., Dietrich, W.E., Torres, R., Anderson, S.P., Heffner, J.T., and Loague, K., 1997, Hydrologic response of a steep, unchanneled valley to natural and applied rainfall: Water Resources Research, v. 33, p. 91–109.

Pavich, M.J., 1986, Processes and rates of saprolite production and erosion on a foliated granitic rock of the Virginia Piedmont, *in* Colman, S.M., and Dethier, D.P., Rates of chemical weathering of rocks and minerals: Orlando, Florida, Academic Press, p. 551–590.

Personius, S.F., 1993, Age and origin of fluvial terraces in the central Coast Range, western Oregon: U.S. Geological Survey Bulletin Report B 2038, 56 p.

Personius, S.F., Kelsey, H.M., and Grabau, P.C., 1993, Evidence for regional stream aggradation in the central Oregon Coast Range during the Pleistocene–Holocene transition: Quaternary Research, v. 40, p. 297–308.

Raymo, M.E., and Ruddiman, W.F., 1992, Tectonic forcing of late Cenozoic climate: Nature, v. 359, p. 117–122.

Raymo, M.E., Ruddiman, W.F., and Froelich, P.N., 1988, Influence of late Cenozoic mountain building on ocean geochemical cycles: Geology, v. 16, p. 649–653.

Reneau, S.L., and Dietrich, W.E., 1991, Erosion rates in the southern Oregon Coast Range: Evidence for an equilibrium between hillslope erosion and sediment yield: Earth Surface Processes and Landforms, v. 16, p. 307–322.

Reneau, S.L., Dietrich, W.E., Rubin, M., Donahue, D.J., and Jull, A.J.T., 1989, Analysis of hillslope erosion rates using dated colluvial deposits: Journal of Geology, v. 97, p. 45–63.

Riebe, C.S., Kirchner, J.W., Granger, D.E., and Finkel, R.C., 2001, Strong tectonic and weak climatic control of long-term chemical weathering rates: Geology, v. 29, p. 511–514.

Rosenbloom, N.A., and Anderson, R.S., 1994, Hillslope and channel evolution in a marine terraced landscape, Santa-Cruz, California: Journal of Geophysical Research, v. 99B, p. 14013–14029.

Ruddiman, W.F., and Prell, W.L., 1997, Introduction to the uplift-climate connection, *in* Ruddiman, W.F., ed., Tectonic uplift and climate change: New York, Plenum Press, p. 3–15.

Small, E.E., Anderson, R.S., and Hancock, G.S., 1999, Estimates of the rate of regolith production using Be-10 and Al-26 from an alpine hillslope: Geomorphology, v. 27, p. 131–150.

Stallard, R.F., 1985, River chemistry, geology, geomorphology, and soils in the Amazon and Orinoco basins, *in* Drever, J.I., ed., The chemistry of weathering: Dordrecht, Netherlands, D. Reidel Publishing Company, p. 293–316.

Stallard, R.F., 1992, Tectonic processes, continental freeboard, and the rate-controlling step for continental denudation, *in* Butcher, S.S., Charlson, R.J., Orians, G.H., and Wolfe, G.V., eds., Global biogeochemical cycles: London, UK, Academic Press, p. 93–121.

Stallard, R.F., 1995a, Relating chemical and physical erosion, *in* White, A.F., and Brantley, S.L., eds., Chemical weathering rates of silicate minerals: Mineralogical Society of America Reviews in Mineralogy, v. 31, p. 543–564.

Stallard, R.F., 1995b, Tectonic, environmental, and human aspects of weathering and erosion: A global review using a steady-state perspective: Annual Review of Earth and Planetary Sciences, v. 23, p. 11–39.

Stonestrom, D.A., White, A.F., and Akstin, K.C., 1998, Determining rates of chemical weathering in soils—Solute transport versus profile evolution: Journal of Hydrology, v. 209, p. 331–345.

Swank, W.T., Vose, J.M., and Elliott, K.J., 2001, Long-term hydrologic and water quality responses following commercial clearcutting of mixed hardwoods on a southern Appalachian catchment: Forest Ecology and Management, v. 143, p. 163–178.

Torres, R., Dietrich, W.E., Loague, K., Montgomery, D.R., and Anderson, S.P., 1998, Unsaturated zone processes and the hydrologic response of a steep, unchanneled catchment: Water Resources Research, v. 34, p. 1865–1879.

White, A.F., Blum, A.E., Schulz, M.S., Huntington, T.G., Peters, N.E., and Stonestrom, D.A., 2002, Chemical weathering of the Panola granite: Solute and regolith elemental fluxes and the weathering rate of biotite, *in* Hellmann, R., and Wood, S.A., eds., Water rock interaction, ore deposits, and environmental geochemistry, a tribute to David A. Crerar: Geochemical Society Special Publication 7, p. 37–59.

White, A.F., and Blum, A.E., 1995, Effects of climate on chemical weathering in watersheds: Geochimica et Cosmochimica Acta, v. 59, p. 1729–1747.

White, A.F., Blum, A.E., Schulz, M.S., Vivit, D.V., Stonestrom, D.A., Larson, M., Murphy, S.F., and Eberl, D., 1998, Chemical weathering in a tropical watershed, Luquillo Mountains, Puerto Rico: I. Long-term versus short-term weathering fluxes: Geochimica et Cosmochimica Acta, v. 62, p. 209–226.

White, A.F., Bullen, T.D., Schulz, M.S., Blum, A.E., Huntington, T.G., and Peters, N.E., 2001, Differential rates of feldspar weathering in granitic regoliths: Geochimica et Cosmochimica Acta, v. 65, p. 847–869.

Worona, M.A., and Whitlock, C., 1995, Late Quaternary vegetation and climate history near Little Lake, Central Coast Range, Oregon: Geological Society of America Bulletin, v. 107, p. 867–876.

MANUSCRIPT RECEIVED BY THE SOCIETY APRIL 20, 2001
REVISED MANUSCRIPT RECEIVED JANUARY 2, 2002
MANUSCRIPT ACCEPTED JANUARY 21, 2002

Printed in the USA